Laser Physics Letters

Astro Ltd.

LETTER

Use of laser-induced bubbles in intraocular pressure measurement: a preliminary study

To cite this article: Fatih Altindis *et al* 2019 *Laser Phys. Lett.* **16** 015601

IOP Publishing | Astro Ltd Laser Physics Letters
Laser Phys. Lett. **16** (2019) 015601 (11pp) https://doi.org/10.1088/1612-202X/aaeda6

Letter

Use of laser-induced bubbles in intraocular pressure measurement: a preliminary study

Fatih Altindis[1,2], Ibrahim T Ozdur[1], Sait N Mutlu[3] and Bulent Yilmaz[1,2,4,5]

[1] Electrical-Electronics Engineering Department, Abdullah Gül University, Kayseri, Turkey
[2] Kornea Biomedical and Optical Systems LLC, Kayseri, Turkey
[3] Maya Ophthalmology Hospital, Kayseri, Turkey

E-mail: bulent.yilmaz@agu.edu.tr

Received 20 September 2018
Accepted for publication 23 October 2018
Published 23 November 2018

Abstract

This work investigates the feasibility of a novel approach for measuring intraocular pressure (IOP) by analyzing micron-level laser-induced bubble characteristics in the intraocular fluid. We believe that this concept may be used as a non-invasive alternative for measuring a patient's IOP by analyzing the laser-induced bubble volume in the intraocular fluid in the anterior chamber of the eye. The behavior of laser-induced bubbles was examined under differing fluid pressure levels and at differing laser pulse energy levels. An intraocular medium-like environment was imitated and an imaging system was designed in order to capture laser-induced bubbles with their movements. The video recordings of the bubbles were processed using custom software, and the volume of the bubbles was estimated using three different approaches. The bubble volumes were estimated more accurately by using the rising velocity of the bubble rather than its direct radii appearances on the images. An inversely proportional relationship was observed between the laser-induced bubble volume and the fluid pressure. IOP can be measured with a non-invasive technique using laser-induced bubble volume. Deeper and detailed studies, including clinical studies, may lead to the use of lasers for measuring IOP.

Keywords: laser-induced bubbles, intraocular pressure, bubble physics, digital image processing

(Some figures may appear in colour only in the online journal)

Introduction

The introduction of short-pulse lasers has had breakthrough effects on the treatment of eye problems as it enables non-invasive surgical operations. Laser-assisted *in situ* keratomileusis for the correction of optical defects such as myopia, hyperopia and astigmatism [1], and Nd:YAG laser treatments to remove clouding in lenses (cataracts) are the two examples of short-pulse lasers applications in ophthalmology. However, the laser-based approaches have some disadvantages for patients. After the laser surgery, the patient's cornea becomes very fragile to external impacts due to the energy exposed on it [2, 3]. Thus, some of the routine examination procedures such as intraocular pressure (IOP) measurements become inapplicable for those patients. For instance, IOP measurement devices (ocular tonometers) apply direct physical force or air pressure to the cornea in taking measurements. Even for outpatients, these IOP measurement approaches are extremely uncomfortable [4–6]. In addition, the available methods for measuring IOP may not give accurate results, due to the variant structure of the cornea in terms of thickness and stiffness. Eyes with thick corneas tend to have pressure values that are

[4] Correspondence Address: Abdullah Gül University, Sumer Campus, Kocasinan, Kayseri, Turkey.
[5] Author to whom any correspondence should be addressed.

over-estimated by ocular tonometry, whereas eyes with thin corneas may result in under-estimated values. While short-pulse laser technology is a method of choice in many areas of ocular operations and surgeries [3, 7], it has not been used to measure IOP.

Nd:YAG lasers are able to create micro-sized cavitation bubbles and they are used to examine cavitation bubble physics in many studies. This is accomplished by focusing the laser beam into a fluid and applying high energy to a small portion of the fluid to induce evaporation. This vaporized gas is specifically referred to as a 'cavitation bubble' or 'laser-induced bubble', and its behavior has been investigated in many studies [8–15]. None of these studies focused on the relationship between the cavitation bubble and fluid pressure after it starts rising in the fluid.

In this study we investigated the feasibility of a novel approach to IOP measurement, using laser-induced bubbles. For this purpose, we examined the behavior of laser-induced bubbles under different conditions, which are laser beam energy and fluid pressure level. Increases and decreases in fluid pressure change the laser-induced bubble's volumes that are created with the same energy level of a laser beam. Even though the bubble's volumes are micro-sized, ideally, the change in the bubble volume can be observable and can be used as a basis for measuring the fluid pressure. The laser-induced bubble can be created in the intraocular fluid of the anterior chamber of the eye, and bubbles can be tracked with an imaging system. The volume change of these bubbles can be used to measure the IOP of the eye. To demonstrate the fluid pressure effects on laser-induced bubbles, we prepared an intraocular medium-like environment, and then designed an imaging system in order to record laser-induced bubbles and their movements. Laser-induced bubbles were created for varying fluid pressure levels and recorded with the custom-designed imaging system. The videos were processed frame by frame with a custom-developed image processing algorithm, and the volumes of the bubbles were computed using three different approaches. The relationship was found between fluid pressure in the intraocular-like environment and the bubble volume, and the results are presented in the following sections.

Materials and methods

Laser system

Clinical laser devices include a laser source, guide light, slit illumination unit, and optical microscope. The laser system used in this study (LightMed, LIGHTLas YAG, San Clemente, CA, USA) has been used mostly for capsulotomy and membranectomy at Maya Ophthalmology Hospital in Kayseri, Turkey. Figure 1 shows the laser system, which has a crystal-Q laser cavity technology and a 1064 nm wavelength with 4 ns pulse width. The laser pulse energy range can be tuned from 0.2 mJ to 10 mJ and the pulses can be formed with up to a 45° angle from the center to the left or right. The microscope has magnification options from 5× to 40×. The illumination unit on the device provides slit light on the focus of the laser in order to brighten the application area.

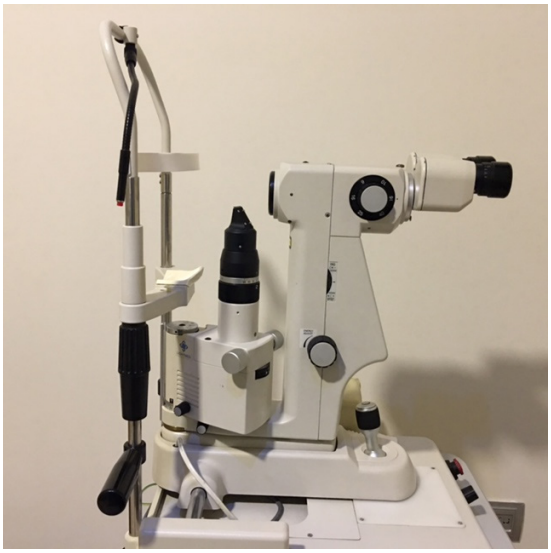

Figure 1. Side view of the laser system used in this study.

Figure 2. Leak-proof cuvette used as an intraocular-like environment.

Intraocular-like environment

The aim of this proof-of-concept study was to show the systematic relationship between the volume of laser-induced bubbles and intraocular-like fluid pressure. Therefore, a leak-proof and transparent intraocular-like environment was designed, with adjustable fluid pressure. For this design, a leak-proof glass cuvette was chosen as the fluid container. It was made of thin transparent glass that did not alter the laser power significantly. The dimensions of the cuvette were 48 × 14 × 14 mm (figure 2).

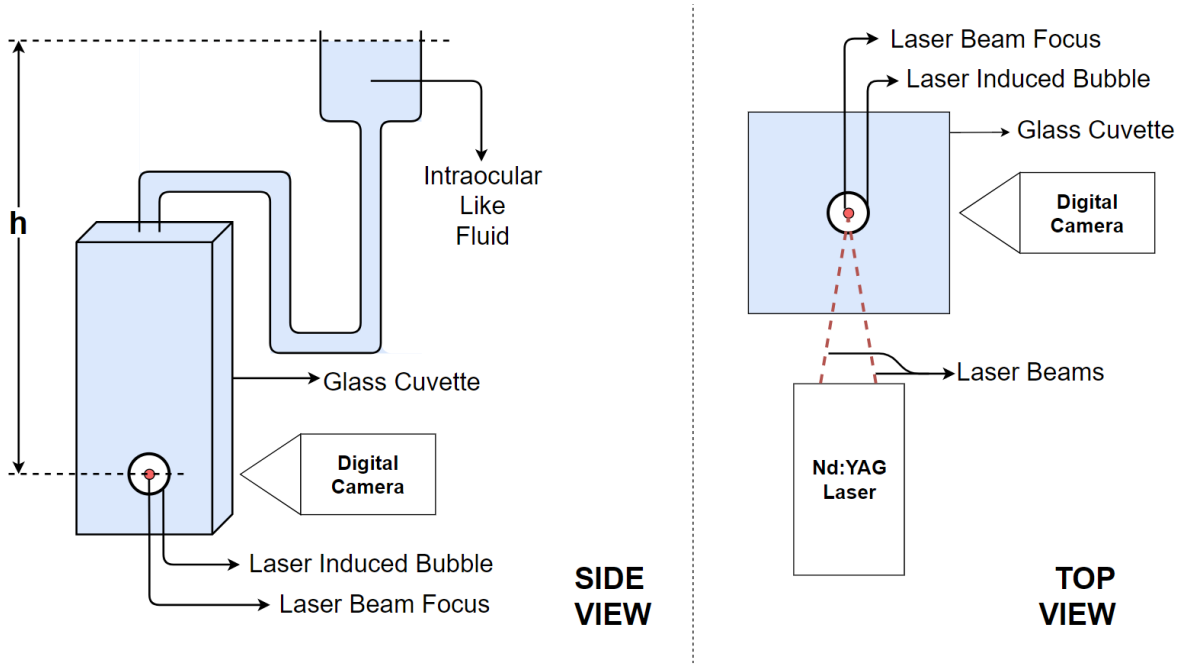

Figure 3. According to Pascal's law, the height difference between the fluid level in the glass cuvette and the fluid container determines the pressure in the fluid.

The cuvette was filled with paraffinum liquidum-based oil that was pure and sterilized from foreign particles. We know that the bubbles rise more slowly in low-density fluids than high-density fluids. Thus, the paraffinum liquidum based oil provided better conditions than water for capturing bubble images, since it has a density of 0.89 gr cm^{-3}. As shown in figure 3, the pressure of the fluid inside the cuvette was adjusted by varying the height difference between the fluid level in the cuvette and the fluid container, as proposed in Pascal's Law.

Imaging system

The imaging system was one of the most important components of this study, as further work relied on images of laser-induced bubbles (LIBs). The imaging system was designed to be stable, fast, and reliable enough to capture micro-sized bubbles. In order to track and capture LIBs accurately, without any blur due to motion or resolution, the digital camera should have a high shutter speed and a high rate of frames per second. The rear camera on an iPhone 7 smartphone was used, with an optical magnifier lens attached to it in order to zoom into LIBs and record them, as shown in figure 4.

The magnification lens was disassembled from another digital microscope camera (TD brand digital industrial microscope with 50 × optic zoom) and attached to the smartphone. The shutter speed of the rear camera was 0.002 s. The LIB images were recorded in the slow motion video recording option that was available on the smartphone. Using this option, it was possible to record videos at 240 frames per second, with which it was possible to capture any volume changes of LIBs while they were rising in the fluid. The videos obtained during our experiments depicted the spherical-shaped bubbles

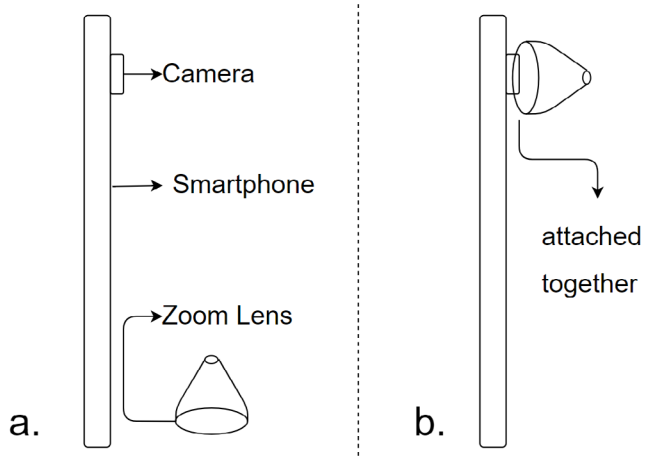

Figure 4. An iPhone 7 and a magnification lens attached via a plastic cover constituted our imaging system.

clearly, as shown in figure 5. In this figure, one can also see the rising of a bubble.

Image processing

LIB images were processed by following the steps shown in figure 6. A custom image-processing approach was implemented to automatically detect the presence of a bubble, its approximate circumference, and its center coordinates. These detected parameters were used to investigate bubble volume characteristics at differing fluid pressure levels.

First, a reference frame was chosen from the recording in order to exclude all irrelevant objects and illumination which were fixed across all frames. The video recording was analyzed frame by frame; each frame was analyzed individually.

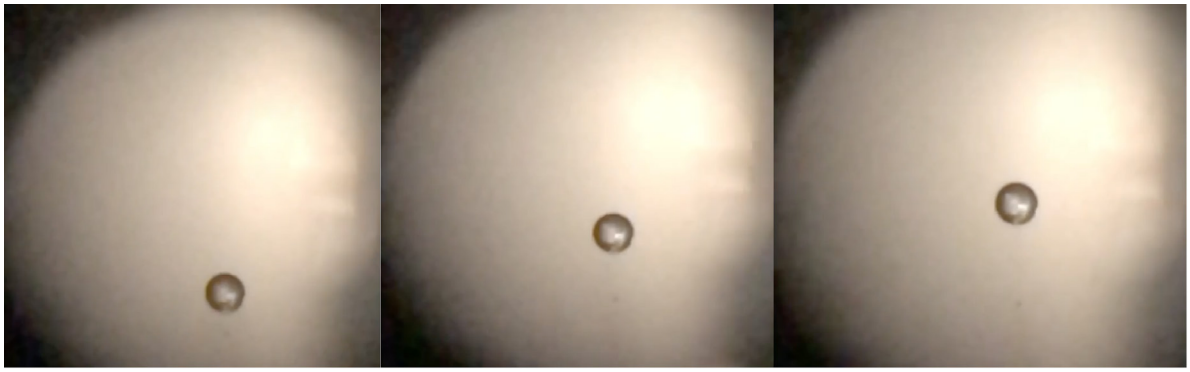

Figure 5. Video images indicating the rising of a bubble in the fluid.

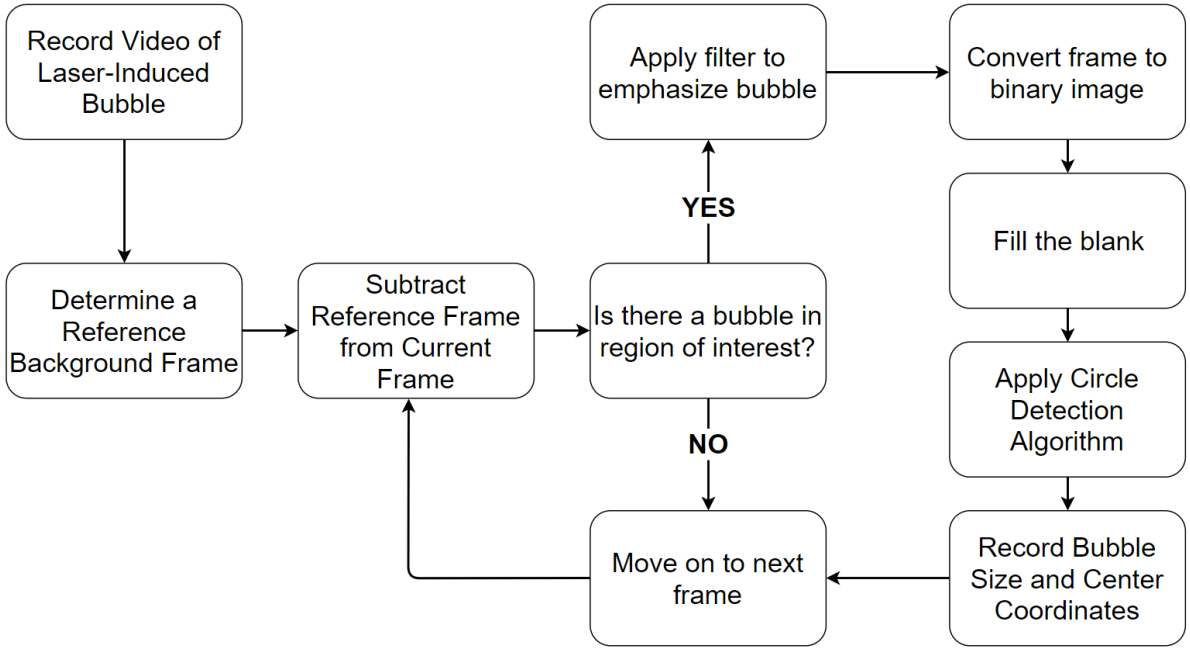

Figure 6. Flow of image processing algorithm for the captured images of laser-induced bubbles.

At each iteration, the initially chosen reference frame was subtracted from the current frame. This operation resulted in a single gray image, which included only the difference between the current frame and the reference frame. The selected reference frame, one sample frame including a laser-induced bubble, and the subtraction result of these two images are demonstrated in figure 7.

When there was a bubble in the predetermined region of interest, the algorithm started applying a series of morphological operations to determine the exact boundaries of the bubble. First, the image was thresholded to highlight faded pixels of the bubble. A circular filter was then applied on the image that emphasized circular objects (the bubble). However, the circular filter also blurred the boundaries of the object. The filtered frame was converted from the gray-scale image to a binary image, and the bubble boundaries were deblurred. Only those pixels where the bubble was present were given a value of 1, and the rest were given a value of zero in this new binary image. If there was a hole in the bubble, it was filled by morphological dilation. This new binary image was taken into the circle detection algorithm, which was a built-in function in MATLAB. This function used the binary image as the input, applied the Hough transform-based circle detection algorithm, and fitted the smallest circle that would cover the white region in the image. The output was then given as the detected circle's center coordinates and radius as a pixel-wise value, if any were detected. When it did not detect any circular objects, it yielded an empty matrix as the output. The last step of the bubble detection algorithm, before it moved to the next frame, was to record the center coordinate values and radius value of the bubble in a matrix. This helped us to look at each bubble's behavior for a certain amount of time. It was also possible to analyze how bubble volume changed while it was rising, and how it was rising in the fluid. Figure 8 shows visual results of each stage of the image processing algorithm for a single frame.

Bubble volume estimation

Laser-induced bubble volumes were computed using two parameters that are extracted during the circle detection process (the radius and coordinates of the circle center). They were used in two different approaches.

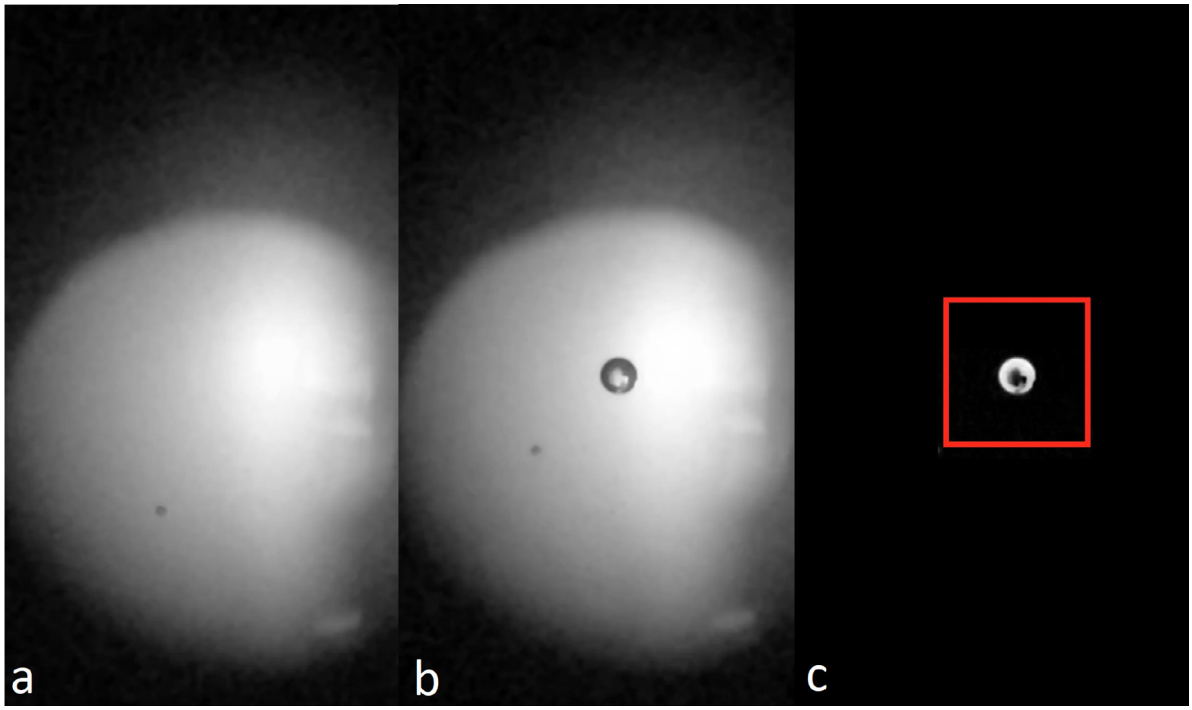

Figure 7. Subtraction result of the frame, with a bubble (b) from the reference frame (a) shown in the right-most panel (c). In the difference frame, the bubble is marked with a red square.

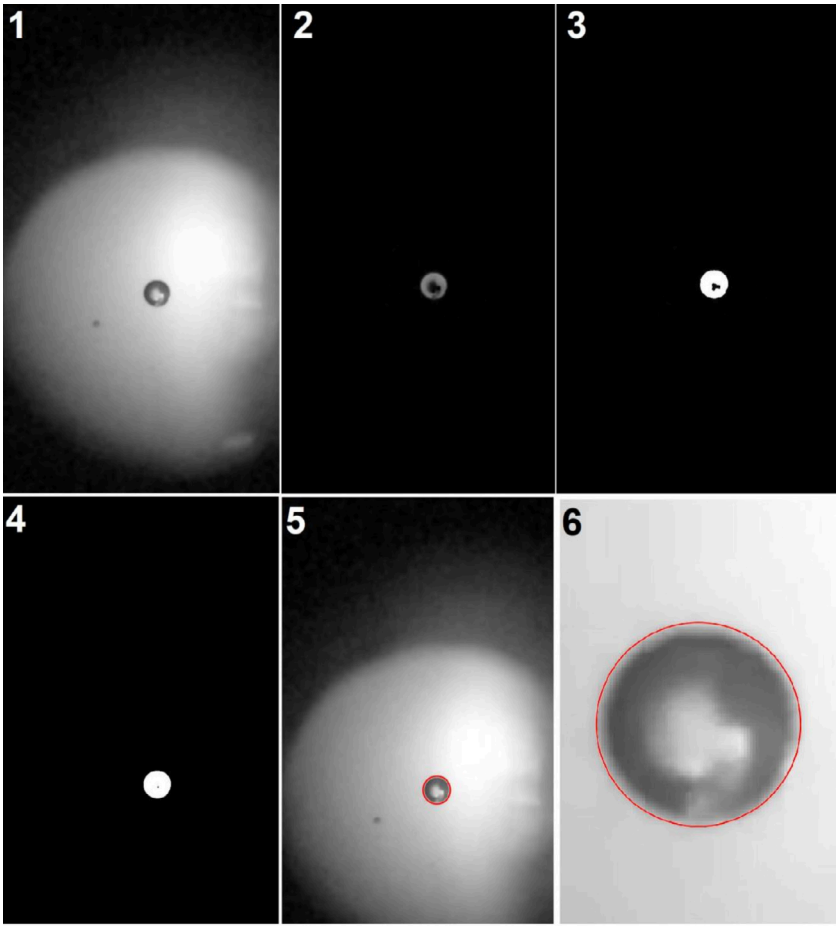

Figure 8. The circle detection steps for a sample frame (1). They depict the difference from the reference (2), its black-and-white version (3), hole-filling result (4), circle-detection in the image (5), and zoomed version of the bubble (6) and the fitted circle in red.

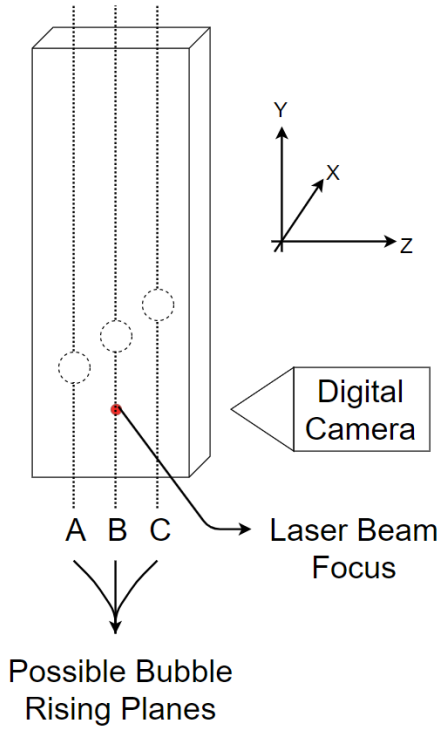

Figure 9. Laser-induced bubbles might rise in different directions even though the laser was aimed at the same focal point. This affected the radius computations of the image-processing algorithm.

The detected radius of the bubble was used to estimate its volume. Since it was a rough estimation based on a 2D projection of the bubble from the camera view, bubble volumes estimated by this method might cause incorrect results for the same fluid pressure level. Bubbles follow different paths, depending on their Reynolds numbers. The Reynolds number of the bubble can be calculated using the following formula, where v_b is the bubble velocity and μ_f is the fluid viscosity [16]:

$$\mathrm{Re} = \frac{v_b 2r}{\mu_f}.$$

If the Reynolds number (Re) of the bubble is less than 1 (Re $<$ 1), then it follows a rectilinear path [17–19]. All-laser induced bubbles followed a rectilinear path as they rose because their Re values were all less than 1, but also they presented on different *x*-*y* planes from the view of the imaging system, as shown in figure 9. This is the reason behind incorrect bubble volume estimations calculated using detected radius values. When they were on planes relatively close to the imaging system, their radii were measured larger than their actual sizes. The exact opposite case also occurred: when they were relatively far away from the imaging system, their radii were measured smaller than their actual sizes. This caused a variation between estimated bubble volumes with the radii-based approach.

Despite the detected radius values being ineffective in estimating bubble volumes accurately enough to quantify fluid pressure changes, an alternative and more challenging method was developed in order to perform more accurate bubble volume estimations from the captured images. Since the center coordinates of the detected bubbles were known, position–time data of the bubble was known as well. The velocity and acceleration of the laser-induced bubbles can be derived by using their position data. Moreover, velocity and acceleration are directly related to the net force that is applied to the bubble, according to Newton's second law of motion ($F = m \cdot a$). The initial velocity of a bubble is zero; hence, its measured velocity depends only on the net force that is effective on the bubble. The net force is equal to the sum of the different potential forces that are effective on the motion of a bubble in a fluid, which are the buoyancy force (F_B), quasi-steady force (F_QS), history (Basset) force (F_H), added-mass force (F_AM), force due to free-stream acceleration (F_FS), and drag force (F_D) [17, 20]. Archimedes' equation ($F = \rho_f \cdot \mathrm{g} \cdot \mathrm{V}$) gives us the buoyancy force, where $V = \frac{4}{3} \cdot \pi \cdot r^3$ and the magnitude of the buoyancy force is related to volume of the bubble, because fluid density and gravity were constant [21–24]. The quasi-steady force, history force, and added-mass force also depend on the volume of the bubble [20, 23]. The equation that consists of the sum of these forces is equal to the net force equation mentioned above. Since we were dealing with bubbles that have very small Reynolds numbers (Re $\ll$ 1) [25], the quasi-steady force and history force are negligibly small and were ignored. Also, there is no fluid flow, so the free-stream force becomes zero. The remaining forces are used to express the net force that is effective on the bubbles ($F_\mathrm{AM} = F_\mathrm{B} + F_\mathrm{D}$) [26].

$$V \cdot (p_f \cdot C_m + p_b) \cdot \frac{dU_b}{dt} = \frac{4}{3} \cdot \pi \cdot r^3 \cdot (p_f - p_b) \cdot g - \frac{\pi r^2}{2} \cdot p_f \cdot C_D \cdot U_b^2.$$

In this equation, C_m is the added mass coefficient which is 0.5 for spherical bubbles, and C_D is the drag coefficient and is calculated using *Re*. There are many proposed methods for the C_D coefficient [27–30]; we used Luo's proposal, where $C_D = \frac{16}{R_e} \cdot \left[1 + 0.15\left(R_e^{0.687}\right)\right]$, because it is a closer approach for LIBs than others. If bubble density (p_b) is neglected because it is negligibly small compared to fluid density (p_f), the formula can be rearranged in order to calculate the radii of the bubbles, and it becomes;

$$r = -\frac{3 \cdot C_D \cdot U_b^2}{4 \cdot \left(\frac{dU_b}{dt} - 2g\right)}.$$

This formula approximates the radius by using the simultaneous velocity and acceleration of the bubble. In addition to using the total sum of these forces for radius calculation, it is possible to calculate the radius of the bubble using Stokes' law [31], or the Hadamard [32] and Rybczynski [33] studies as it was discussed in Aybers and Tapucu [18]. According to Stokes' law, the terminal velocity of a bubble is:

$$U_{b(ST)} = \frac{2r^2 (\rho_f - \rho_b) g}{9\mu}.$$

Hadamard and Rybczynski described the terminal velocity of the bubble as:

$$U_{b(H-R)} = \frac{2r^2\left(\rho_f - \rho_b\right)g}{3\mu} \cdot \frac{\mu + \mu'}{2\mu + 3\mu'},$$

where U_b is the bubble velocity, μ is the fluid viscosity, and μ' is the internal viscosity. This formula can be rearranged by neglecting μ' for our case, since $\mu' \ll \mu$ [25, 34, 35]. The rearranged version of the Hadamard and Rybczynski equation is

$$U_{b(H-R)} = \frac{r^2\left(\rho_f - \rho_b\right)g}{3\mu} = \frac{3}{2}U_{b(ST)}.$$

The bubble speed is already known, and if we rearrange this formula in order to calculate the radius of the bubble from the measured velocity, it becomes:

$$r = \left(\frac{U_b \cdot 3\mu}{\left(\rho_f - \rho_b\right)g}\right)^{\frac{1}{2}}.$$

The main difference of this formula from the previous one is that it is assumed that the bubble speed reached a terminal constant speed, where acceleration is zero. It means that the net force is zero ($0 = F_B + F_D$).

There is another rough radius estimation method which uses only the buoyancy force. It is assumed that net force is equal to the buoyancy force. In this case, two formulas are arranged together to find the radius of the bubble:

$$r = \left(\frac{3 \cdot m \cdot a}{4\pi \cdot \rho_f ro \cdot g}\right)^{1/3}.$$

It is known that acceleration is the second derivative of the position with respect to time, and the bubble position was known since the coordinates of the bubble centers were recorded. Therefore, by using the second derivative of the position of the bubble, the acceleration of the bubble was computed. Since the fluid density and gravitational acceleration were the same for all laser-induced bubbles formed in our experiments, only the acceleration value could give information about the volume of the bubble. This approach was used in order to obtain more accurate results by decreasing the variation in the bubble volume estimation.

It is known that laser-induced bubbles that are formed using the same laser beam energy level are repeatable [36, 37]. Therefore it is expected that under the same fluid pressure, laser-induced bubbles should have equal volumes. However, our measurements revealed that it was nearly impossible to deliver the same amount of energy to laser beams for every single laser shot in our medical laser system, and a small variance of laser beam energy occurs between laser shots due to aged laser cores. This problem was overcome by taking multiple laser shots for each pressure level, and stable records were taken.

Laser pulse energy effect

Laser energy focused on a point causes the formation of plasma and vaporization of the fluid, resulting in a bubble. Thus, the experiment set-up was prepared to investigate the effect of laser energy on LIBs. In order to understand the effect of laser energy, varying energy levels were used to generate the laser-induced bubbles. To perform this analysis, an initial energy level of 0.8 mJ was selected, and it was increased by 0.2 mJ at each step. Four energy levels were used in this part of the study, of 0.8, 1.0, 1.2 and 1.4 mJ. At each energy level, multiple shots (up to 40) were applied, most of which resulted in bubble formation. The 1.0 mJ laser energy level provided the most stable and successful laser shots in terms of generating single bubbles. This allowed us to keep the laser beam energy constant and stable for fluid pressure effect measurements. For each bubble, the video recordings were processed and bubble volumes were computed using a velocity-based estimation approach.

Fluid pressure effect

The most important part of this study was the observation that the laser-induced bubble volumes systematically changed with respect to the fluid pressure inside a container. Theoretically, it was proposed that the bubble volume would decrease with increasing fluid pressure, since the laser-induced bubble radius is dependent on the fluid pressure [24]. In order to prove this theory for the laser-induced bubbles, an experimental set-up was prepared. Experiments were performed under varying levels of zero, 2, 4, and 6 mmHg relative to the atmospheric pressure (760 mmHg). Fluid pressures were obtained by changing the fluid height levels, as shown in figure 3. At each pressure level more than 70 single laser-induced bubbles were formed with 1 mJ laser beam energy, and each recorded bubble was tracked for more than 180 frames (500 ms). We should note that each laser shot generated only one bubble, and that laser shots that generated multiple bubbles were not taken into account. Then, the video recordings processed using the techniques proposed in the bubble volume estimation section. The volumes of each bubble were computed individually, and the values were averaged for every individual pressure level.

Results

In the methods section we mentioned that there were two parameters that affected the bubble volume: laser energy and fluid pressure in the container. Therefore, their effects on the bubble volumes were investigated separately. Also, the performances of the three volume estimation approaches explained above were compared.

First, we investigated the effect of volume estimation approaches, because it is important to know the estimation differences between applied volume estimation approaches. For this purpose, 75 bubbles were created with 1 mJ laser beam energy under the same fluid pressure, and each bubble's volume was estimated by the three approaches. Estimated bubble radius histograms are shown in figure 10. The distribution of estimated bubble volumes shows that all three approaches have different estimation errors, and velocity and force-based approaches yielded more robust (lower variance) results compared to the radii-based approach.

Laser beam energy effects are shown in figure 11; the measured bubble volumes changed for different energy levels.

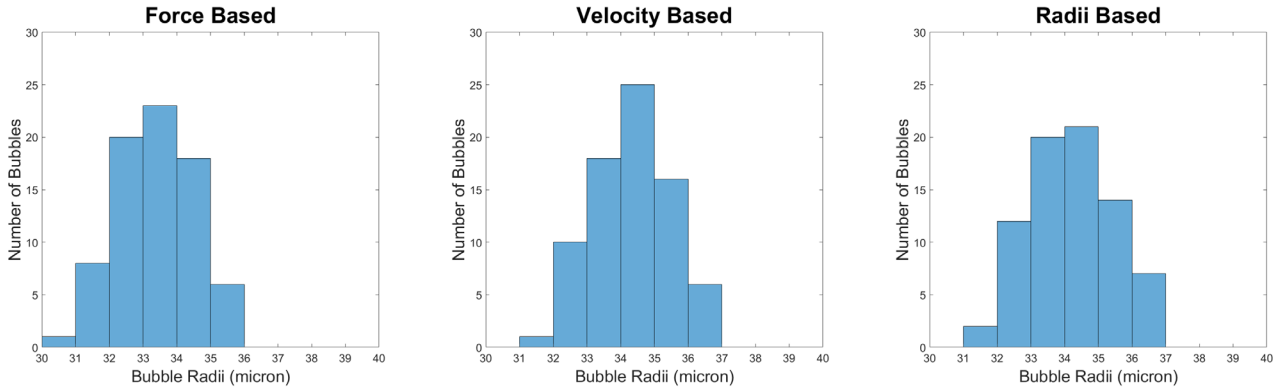

Figure 10. The distribution of the estimated bubble radius for each approach.

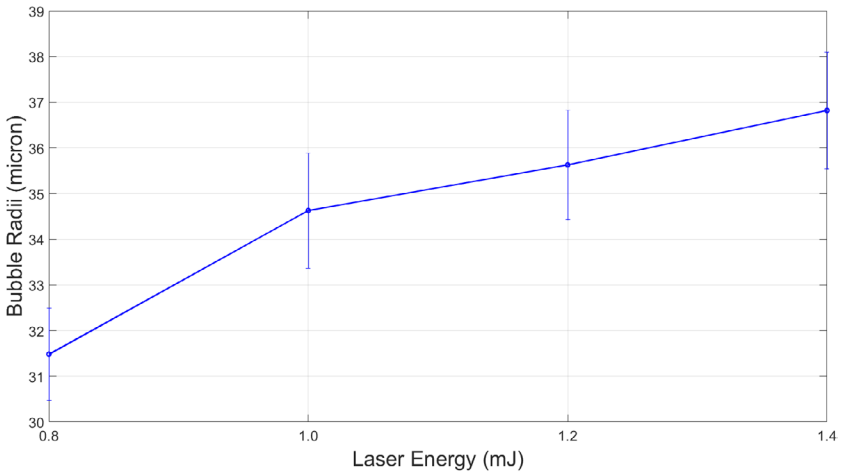

Figure 11. Estimation of laser-induced bubble radius at the same pressure level with four energy levels.

Our experiments indicated that the minimum energy required to form a bubble was about 0.6 mJ per optical pulse. However, we also noticed that it was better to apply a slightly higher energy level to obtain identical bubbles, because the laser core might not deliver the same energy level every time, due to the conditions discussed. This deviation might have prevented the formation of identical bubbles at the minimum energy level (0.6 mJ). As expected, a higher laser beam energy resulted in larger bubble volumes. Higher laser energy causes more fluid evaporation and eventually results in larger bubble volumes. Additionally, identical bubbles were created at higher energy levels, which was important in eliminating the laser beam energy effect and investigating the fluid pressure effect on LIBs. However, the increased laser energy also caused some of the laser bubbles to fragment into smaller bubbles. The reason for this behavior can be explained with the shockwaves emitted after the first collapse. Larger bubbles emitted more powerful shockwaves, which were able to split a bubble into a couple of smaller bubbles. The optimum laser energy for creating a single laser-induced bubble per optical pulse was determined to be 1 mJ, as mentioned above.

The radius estimations of laser-induced bubbles with the three techniques and with respect to the fluid pressure are shown in figure 12. The estimations from force and velocity-based approaches showed that the radii of the bubbles gradually decreased when the fluid pressure increased. The only difference between these two approaches was a difference of 1 μm in the estimated radii values. However, the radii-based approach showed slightly different results. As discussed in the image processing section above, the estimated radius of this approach may vary due to the view of the digital camera, but the force and velocity-based approaches were affected less by the view of the camera, because these approaches estimate the bubble radius from the motion of the bubble rather than its appearance on the images. The results of the radii estimations in figures 10 and 12 proved that force and velocity-based estimations provided more accurate results than radii-based estimations. The most important point from figure 12 is that systematic fluid pressure changes have an observable and quantifiable effect on micro-sized laser-induced bubbles.

Discussion

In this proof of concept study, we aimed to perform preliminary research into solving the problem of measuring intraocular pressure that ophthalmology clinicians have been encountering frequently. This new technique aims to measure intraocular pressure by using laser-induced bubbles, which are formed in the anterior chamber of the eye. This study was

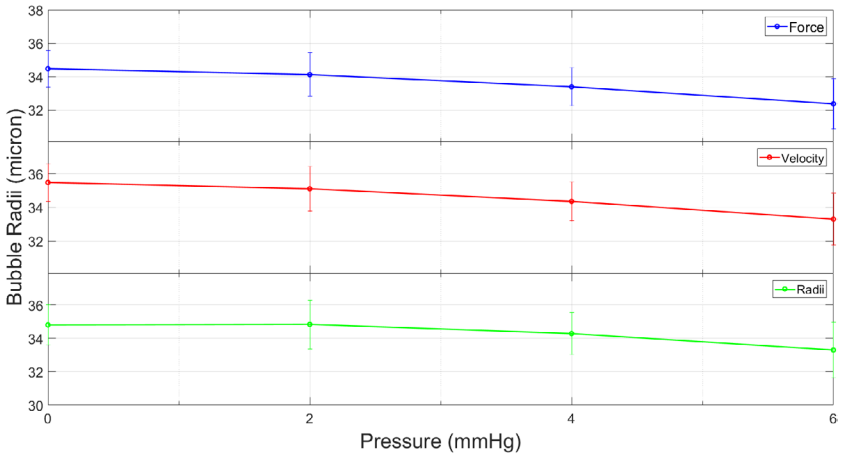

Figure 12. Estimation of laser-induced bubble volumes at the same pressure level, with four pressure levels.

inspired by previous studies in which the researchers investigated the behaviors and characteristics of both air bubbles and laser-induced bubbles in various fluids [13, 31, 36–44].

Available intraocular pressure measurement devices (tonometers) measure the change of resilience of the cornea or sclera. However, it is known that resilience depends on thickness and corrosion, besides the intraocular pressure. Thus, these tonometers cannot measure intraocular pressure precisely, and the measured values must be corrected using a table that takes account of the corneal thickness. Besides that, laser surgeries alter the physical structure of the eye, and this alteration causes failure of intraocular pressure measurement with a tonometer.

In this study, it is proposed that laser-induced bubble volumes depend on the fluid internal pressure and laser beam energy. Laser-induced bubbles that are created with the same energy level but under different fluid pressure levels have different volumes. The bubble volume or the change in bubble volume might provide information about the internal fluid pressure. In order to prove this concept, we have performed experimental studies. Two parameters (laser beam energy and fluid pressure) that affect the volume of a LIB were varied, in order to observe how these parameters affected the laser-induced bubbles' volume and movement characteristics.

In order to understand the effect of internal fluid pressure, the other parameter (laser beam energy) was fixed, and only the internal fluid pressure was changed during the measurements. The results showed that the fluid pressure had a noteworthy effect on laser-induced bubble volumes, and this volume–pressure relationship could be measured with the laser system and the imaging set-up. The cornerstone of the study was to measure the bubble radii as accurately as possible. For this purpose, bubble motion was observed and bubble radii were estimated using the motion of the bubble inside the fluid. Even though for simplicity the estimations ignored some of the parameters, such as bubble gas density, history force, diffusion, and condensation of the vapor bubble, the results showed that the bubble estimation approaches performed well enough to differentiate a gradual increase or decrease of fluid pressure. Despite the ignored parameters, 2 mmHg fluid pressure resolutions had an observable effect on bubble radius estimations, and these measurements were not affected by any parameter other than the fluid pressure. This outcome is the most important result of the study, since the proposal of this study was proved under experimental conditions, and quantitative fluid pressure changes can be estimated from the radii of the laser induced-bubbles.

Laser-induced bubbles were created by a Nd:YAG laser device that was already available for capsulotomy operations. Thus, any concerns or side effects of the laser on cornea tissues can be predicted from previous studies in this area [2, 3, 45–47]. But it is certain that vivo experiments should be undertaken in order to understand any possible side effects of this method on cornea tissue. Additionally, due to the discussed technical limitations of the laser device (aged laser core), we were not able to take more precise and more sensitive measurements. But it is possible to obtain more sensitive measurements with better laser systems. At this point, the results in figure 12 show that the internal fluid pressure could be determined by measuring the volume of the laser-induced bubbles that were formed in the fluid.

In addition, one of the important findings of this study was that while small changes in a roughly estimated radius value dramatically affected volume computations, due to variations in rising planes, radius estimations using the center coordinates of the detected bubble did not vary greatly, even if they moved closer to or further away from the imaging system. Thus, the radius values derived from the rising speed of the bubbles provided more accurate results.

Previous studies mostly focused on the first occurrence of laser-induced bubbles and their maximum size after the first occurrence [10, 13]. One of the factors that affects the maximum size of a bubble during its enlargement phase is the fluid pressure. Fluid pressure is used to calculate the maximum size that the laser-induced bubbles can reach, but in this study this parameter was investigated by observing the bubble volume after it stopped collapsing and enlarging. Our results showed even after the first enlargement and collapse of the bubble, its volume depends on the fluid pressure, and LIB volumes decreased as the fluid pressure increased.

The findings of this study will be the basis for further studies about developing a LIB-based measurement method for

intraocular pressure. Further studies will reveal more about whether this method can substitute the current methods of measuring IOP, but the results of this study strongly promise that the use of LIBs to measure intraocular pressure is feasible.

Acknowledgment

This study was supported by a grant from TÜBİTAK 1512 program with project number 2150492.

Financial Support: TUBITAK, Ankara, 1512, 2150492.

The sponsor or funding organization had no role in the design or conduct of this research.

Conflict of Interest: No conflicting relationship exists for any author.

References

[1] Buratto L and Brint F S 1998 *LASIK Principles and Techniques* (Thorofare, NJ: Slack)
[2] Kerr Muir M G and Sherrard E S 1985 Damage to the corneal endothelium during Nd/YAG photodisruption *Br. J. Ophthalmol.* **69** 77–85
[3] Puliafito C A and Steinert R F 1984 Short-pulsed Nd:YAG laser microsurgery of the eye: biophysical considerations *IEEE J. Quantum Electron.* **20** 1442–8
[4] Han K E, Kim H, Kim N R, Jun I, Kim E K and Kim T I 2013 Comparison of intraocular pressures after myopic laser-assisted subepithelial keratectomy: tonometry-pachymetry, Goldmann applanation tonometry, dynamic contour tonometry, and noncontact tonometry *J. Cataract Refract. Surg.* **39** 888–97
[5] Mardelli P G, Piebenga L W, Whitacre M M and Siegmund K D 1997 The effect of excimer laser photorefractive keratectomy on intraocular pressure measurements using the Goldmann applanation tonometer *Ophthalmology* **104** 945–8
[6] Sánchez-Navés J, Furfaro L, Piro O and Balle S 2008 Impact and permanence of LASIK-induced structural changes in the cornea on pneumotonometric measurements: contributions of flap cutting and stromal ablation *J. Glaucoma* **17** 611–8
[7] Vogel A, Hentschel W, Holzfuss J and Lauterborn W 1986 Cavitation bubble dynamics and acoustic transient generation in ocular surgery with pulsed neodymium:YAG lasers *Ophthalmology* **93** 1259–69
[8] Akhatov I, Lindau O, Topolnikov A, Mettin R, Vakhitova N and Lauterborn W 2001 Collapse and rebound of a laser-induced cavitation bubble *Phys. Fluids* **13** 2805–19
[9] Bloembergen N 1974 Laser induced electric breakdown in solids *IEEE J. Quantum Electron.* **10** 375–86
[10] Brennen C E 2013 *Cavitation and Bubble Dynamics* (Cambridge: Cambridge University Press)
[11] Byun K T and Kwak H Y 2004 A model of laser-induced cavitation *Japan. J. Appl. Phys.* **43** 621–30
[12] Kennedy P K, Hammer D X and Rockwell B A 1997 Laser-induced breakdown in aqueous media *Prog. Quantum Electron.* **21** 155–248
[13] Lauterborn W and Ohl C D 1997 Cavitation bubble dynamics *Ultrason. Sonochem.* **4** 65–75
[14] Quinto-Su P A, Venugopalan V and Ohl C-D 2008 Generation of laser-induced cavitation bubbles with a digital hologram *Opt. Express* **16** 18964–9
[15] Ren X D *et al* 2016 Experimental investigation on dynamic characteristics and strengthening mechanism of laser-induced cavitation bubbles *Ultrason. Sonochem.* **32** 218–23
[16] Shew W L, Poncet S and Pinton J F 2006 Force measurements on rising bubbles *J. Fluid Mech.* **569** 51–60
[17] Park W C, Klausner J F and Mei R 1995 Unsteady forces on spherical bubbles *Exp. Fluids* **19** 167–72
[18] Aybers N M and Tapucu A 1969 The motion of gas bubbles rising through stagnant liquid *Wärme Stoffübertragung* **2** 118–28
[19] Aybers N M and Tapucu A 1969 Studies on the drag and shape of gas bubbles rising through a stagnant liquid *Wärme Stoffübertragung* **2** 171–7
[20] Mei R, Klausner J F and Lawrence C J 1994 A note on the history force on a spherical bubble at finite Reynolds number *Phys. Fluids* **6** 418–20
[21] Legendre D and Magnaudet J 1997 A note on the lift force on a spherical bubble or drop in a low-Reynolds-number shear flow *Phys. Fluids* **9** 3572–4
[22] Legendre D and Magnaudet J 1998 The lift force on a spherical bubble in a viscous linear shear flow *J. Fluid Mech.* **368** 81–126
[23] Mei R and Klausner J F 1994 Shear lift force on spherical bubbles *Int. J. Heat Fluid Flow* **15** 62–5
[24] Rayleigh L 1917 VIII. On the pressure developed in a liquid during the collapse of a spherical cavity *Phil. Mag.* **34** 94–8
[25] Parkinson L, Sedev R, Fornasiero D and Ralston J 2008 The terminal rise velocity of 10–100 μm diameter bubbles in water *J. Colloid Interface Sci.* **322** 168–72
[26] Manica R, Klaseboer E and Chan D Y C 2015 Force balance model for bubble rise, impact, and bounce from solid surfaces *Langmuir* **31** 6763–72
[27] Loth E 2008 Quasi-steady shape and drag of deformable bubbles and drops *Int. J. Multiph. Flow* **34** 523–46
[28] Magnaudet J and Legendre D 1998 The viscous drag force on a spherical bubble with a time-dependent radius *Phys. Fluids* **10** 550–4
[29] Takemura F, Takagi S, Magnaudet J and Matsumoto Y 2002 Drag and lift forces on a bubble rising near a vertical wall in a viscous liquid *J. Fluid Mech.* 2002
[30] Luo X, Zhang J, Tsuchiya K and Fan L-S 1997 On the rise velocity of bubbles in liquid–solid suspensions at elevated pressure and temperature *Chem. Eng. Sci.* **52** 3693–9
[31] Stokes G G 1851 On the effect of the internal friction of fluids on the motion of pendulums *Mathematical and Physical Papers* (Cambridge: Cambridge University Press) pp 1–10
[32] Hadamard J 1911 Mouvement permanent lent d'une sphere liquide et visqueuse dans un liquide visqueux *C. R. Hebd. Seances Acad. Sci.* **152** 1735
[33] Rybczynski W 1911 Über die fortschreitende Bewegung einer flüssigen Kugel in einem zähen Medium *Bull. Acad. Sci. Cracovie* **A** 40–6
[34] Allen H S 1900 XXXI. The motion of a sphere in a viscous fluid *London Edinburgh Dublin Phil. Mag. J. Sci.* **50** 323–38
[35] Duineveld P C 1995 The rise velocity and shape of bubbles in pure water at high Reynolds number *J. Fluid Mech.* **292** 325–32
[36] Toker G, Bulatov V, Kovalchuk T and Schechter I 2009 Micro-dynamics of optical breakdown in water induced by nanosecond laser pulses of 1064 nm wavelength *Chem. Phys. Lett.* **471** 244–8
[37] Tomita Y and Shima A 1990 High-speed photographic observations of laser-induced cavitation bubbles in water *Acta Acust. United Acust.* **71** 161–71
[38] Vogel A, Busch S and Parlitz U 1996 Shock wave emission and cavitation bubble generation by picosecond and nanosecond optical breakdown in water *J. Acoust. Soc. Am.* **100** 148–65
[39] Prosperetti A 2004 Bubbles *Phys. Fluids* **16** 1852–65
[40] Lee S J and Kim S 2005 Simultaneous measurement of size and velocity of microbubbles moving in an opaque tube using an x-ray particle tracking velocimetry technique *Exp. Fluids* **39** 490–5

[41] Brujan E-A, Nahen K, Schmidt P and Vogel A 2001 Dynamics of laser-induced cavitation bubbles near an elastic boundary *J. Fluid Mech.* **433** 251–81
[42] Gilmore F R 1952 The growths or collapse of a spherical bubble in a viscous compressible liquid *Report* Hydrodynamics Laboratory California Institute of Technology
[43] Ganguli A A, Pandit A B and Joshi J B 2012 Bubble dynamics of a single condensing vapor bubble from vertically heated wall in subcooled pool boiling system: experimental measurements and CFD simulations *Int. J. Chem. Eng.* **2012** 712986
[44] Fujimoto J G, Lin W Z, Ippen E P, Puliafito C A and Steinert R F 1985 Time-resolved studies of Nd:YAG laser-induced breakdown: plasma formation, acoustic wave generation, and cavitation *Investig. Ophthalmol. Vis. Sci.* **26** 1771–7
[45] Hutson M S and Ma X 2007 Plasma and cavitation dynamics during pulsed laser microsurgery *in vivo Phys. Rev. Lett.* **99** 158104
[46] Vogel A and Lauterborn W 1988 Acoustic transient generation by laser-produced cavitation bubbles near solid boundaries *J. Acoust. Soc. Am.* **84** 719–31
[47] Song W D, Hong M H, Lukyanchuk B and Chong T C 2004 Laser-induced cavitation bubbles for cleaning of solid surfaces *J. Appl. Phys.* **95** 2952–6